Published in IET Optoelectronics
Received on 14th December 2007
Revised on 21st August 2008
doi: 10.1049/iet-opt.2007.0095

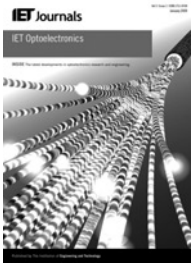

ISSN 1751-8768

High-speed electroabsorption modulation of composite-resonator vertical-cavity lasers

C. Chen[1] *P.O. Leisher*[2] *D.M. Grasso*[3] *C. Long*[1]
K.D. Choquette[1]

[1]*Department of Electrical and Computer Engineering, Micro and Nanotechnology Laboratory, University of Illinois at Urbana-Champaign, 208 N. Wright Street, Urbana, IL 61801, USA*
[2]*nLight Corporation in Vancouver, WA 98665, USA*
[3]*Coherent, Inc., Bridgeton, MO 63044, USA*
E-mail: chenchen@uiuc.edu

Abstract: The high-speed characteristics of a composite-resonator vertical-cavity laser (CRVCL) under both small- and large-signal electroabsorption modulation are investigated. The maximum −3 dB modulation bandwidth of 12.5 GHz is measured. The theoretical modulation response of the CRVCL is derived from the standard rate equations, and the qualitative form is in agreement with the measured results. The CRVCL under electroabsorption modulation exhibits a promising potential to extend the modulation bandwidth beyond that of a conventional VCSEL. However, the CRVCL under large-signal electroabsorption modulation is limited to low data rates, and the large relaxation oscillation resonance must be suppressed for higher-speed digital–optical link applications.

1 Introduction

Vertical-cavity surface-emitting lasers (VCSELs) have emerged as a dominant light source for short-haul high-speed optical data communication and board-to-board optical interconnection applications. VCSELs are attractive in these applications because of their wafer-scale manufacturability, ease of packaging, the ability to fabricate two-dimensional laser arrays and inherent high-speed modulation [1]. Driven by emerging optical networking applications, there is a need to incorporate additional functionalities and flexibility to optoelectronic and photonic devices via higher levels of device integration. For edge-emitting lasers, the coupled-cavity laser structure has been used to obtain single longitudinal mode operation and wavelength tunability [2–4]. Moreover, this idea has been extended into VCSEL design through vertical integration, which has led to the composite-resonator vertical-cavity laser (CRVCL) [5–16]. The CRVCL has demonstrated additional functionalities and flexibility over a conventional VCSEL which have made it successful in many applications, including picosecond pulse generation [8], high-contrast optical switching [10], high single-mode power [11], wavelength division multiplexing [13] and polarisation switching [14].

Recently, the CRVCL has exhibited the potential to extend VCSEL modulation to higher speeds [16]. The CRVCL has the unique ability to change the photon density by varying the gain or absorption in one cavity when fixing the current injection into the other cavity [8, 12, 15, 16]. As a result, this property can enable novel modulation schemes. In the conventional direct modulation of a CRVCL, the modulation of the current density is introduced into one cavity, whereas the current injection into the other cavity is fixed. This results in the modulation of the carrier density, gain and eventually the light output. However, modulation of a CRVCL can also be done in a different way. As the two cavities of the CRVCL are optically coupled, by modulating reverse voltage bias across one cavity, the light output of the CRVCL can be modulated owing to the effect of electroabsorption modulation. This modulation scheme requires that the CRVCL can achieve lasing threshold with current injection into a single cavity [17].

In this paper, we first describe the fabrication process and high-speed measurement of the CRVCL. Second, the theoretical small-signal electroabsorption modulation response of the CRVCL is obtained based on a standard rate equation approach. We then demonstrate the high-speed characteristics of the CRVCL under both small- and large-signal electroabsorption modulation and compare with our simulations. Finally, the challenges for deployment of the CRVCL in optical link applications are discussed.

2 Experiment

The CRVCL in this work is grown by metal-organic chemical vapour deposition. It is composed of a monolithic bottom p-type-distributed Bragg reflector (DBR) with 36 periods, a middle n-type DBR with 12 periods and an upper p-type DBR with 22 periods. The middle DBR mirrors separate two identical optical cavities, each of which contains five $GaAs/Al_{0.2}Ga_{0.8}As$ quantum wells emitting nominally at 850 nm. Owing to the optical coupling through the middle DBR, the CRVCL structure supports two longitudinal cavity modes [6, 7], which correspond to two resonances at 858.3 and 869.5 nm in its reflectance spectrum. The wavelength splitting between the cavity modes is dictated by the number of the middle DBR periods.

The device fabrication begins with the deposition of top ohmic (Ti/Au) ring contacts on the sample surface and the deposition of a broad-area ohmic (Ti/Au) contact on the backside of the sample. SiO_2 is deposited by plasma-enhanced chemical vapour deposition and the upper mesa mask is photolithographically patterned and transferred to the oxide mask using reactive ion etching (RIE). The upper mesas of size approximately $40 \times 40\ \mu m^2$ are then etched using an inductively coupled plasma (ICP)-RIE through the top DBR and half of the middle DBR, and ohmic (AuGe/Ni/Au) ring contacts are then formed. To ensure good conductivity through middle ring contacts, the upper mesa etch must be precisely stopped on a low Al-content mirror layer to avoid forming an oxide barrier, and thus the etching must be carefully controlled by *in situ* optical reflectometry [1]. Additional SiO_2 is then deposited by PEVCD, and lower mesas are photolithographically patterned and transferred to the oxide mask using RIE. Then the lower mesas of size approximately $100 \times 100\ \mu m^2$ are etched by ICP-RIE into the bottom p-type DBR. Subsequently, an oxide aperture is formed for the bottom cavity using selective oxidation [1]. The device used in this work has an oxide aperture of $3 \times 3\ \mu m^2$. In order to facilitate on-wafer high-speed measurement, ground-signal–ground coplanar waveguide contacts for the top cavity are deposited onto cured photo-definable polyimide. The resulting device cross-section and scanning electron microscope image are shown in Fig. 1.

Prior to the high-speed measurement, the continuous-wave characteristics of the CRVCL are obtained using on-wafer probing at room temperature. In Fig. 2*a*, we show the light output against the bottom cavity current (L–I relationship)

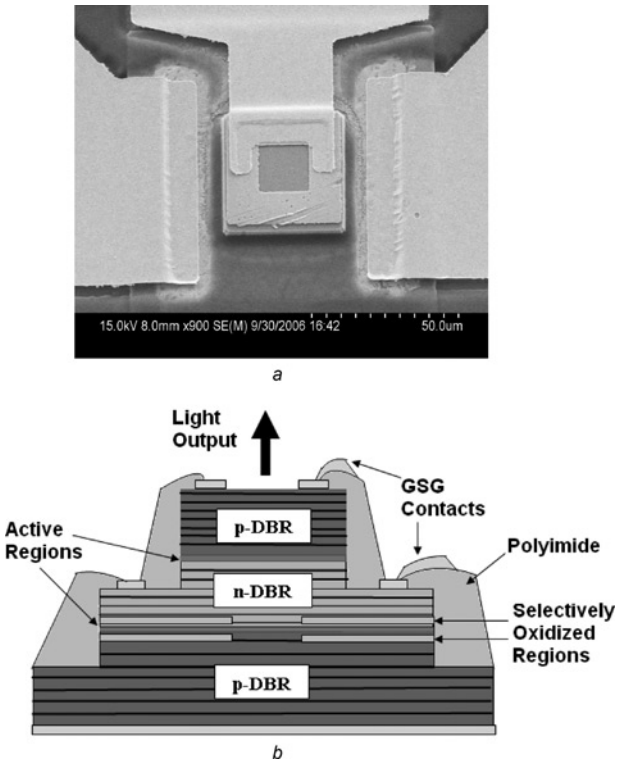

Figure 1 *Device cross-section and image of the scanning electron microscope*

a Scanning electron microscope image of a CRVCL
b Schematic of a CRVCL used for intracavity electroabsorption modulation

for different applied voltages across the top cavity. It is known that varying the top cavity voltage can contribute to both electroabsorption and electrorefraction effects, resulting in changes in the intensity and longitudinal distribution of the lasing mode [18–21]. In this particular CRVCL shown in Fig. 2*a*, the threshold current always increases and light output decreases as larger reverse voltage (or smaller forward voltage) is applied to the top cavity. The increasing threshold current with decreasing output light is consistent with electroabsorption being the dominate effect. The kink in the L–I curve in Fig. 2*a* when the top cavity voltage is 0.75 V corresponds to the transition of lasing from the shorter to the longer wavelength longitudinal cavity mode.

The DC characteristic can also be shown in Fig. 2*b*, which illustrates the light output when the bottom cavity is injected with current when varying the applied voltage across the top cavity. From the electrical behaviour of the top cavity, it can also be considered as a reverse-biased photodetector as the photocurrent is generated shown in Fig. 2*c*. However, it is worthwhile to note that the photodetector efficiency varies with the top cavity voltage in Fig. 2*c*, which causes deviation from the otherwise linear relationship between photon density and photocurrent. Fig. 2*d* illustrates that the single-mode (greater than 30 dB side mode suppression ratio) emission is achieved as a result of the small oxide aperture. The lasing wavelength corresponds to the longer wavelength longitudinal cavity mode.

doi: 10.1049/iet-opt.2007.0095

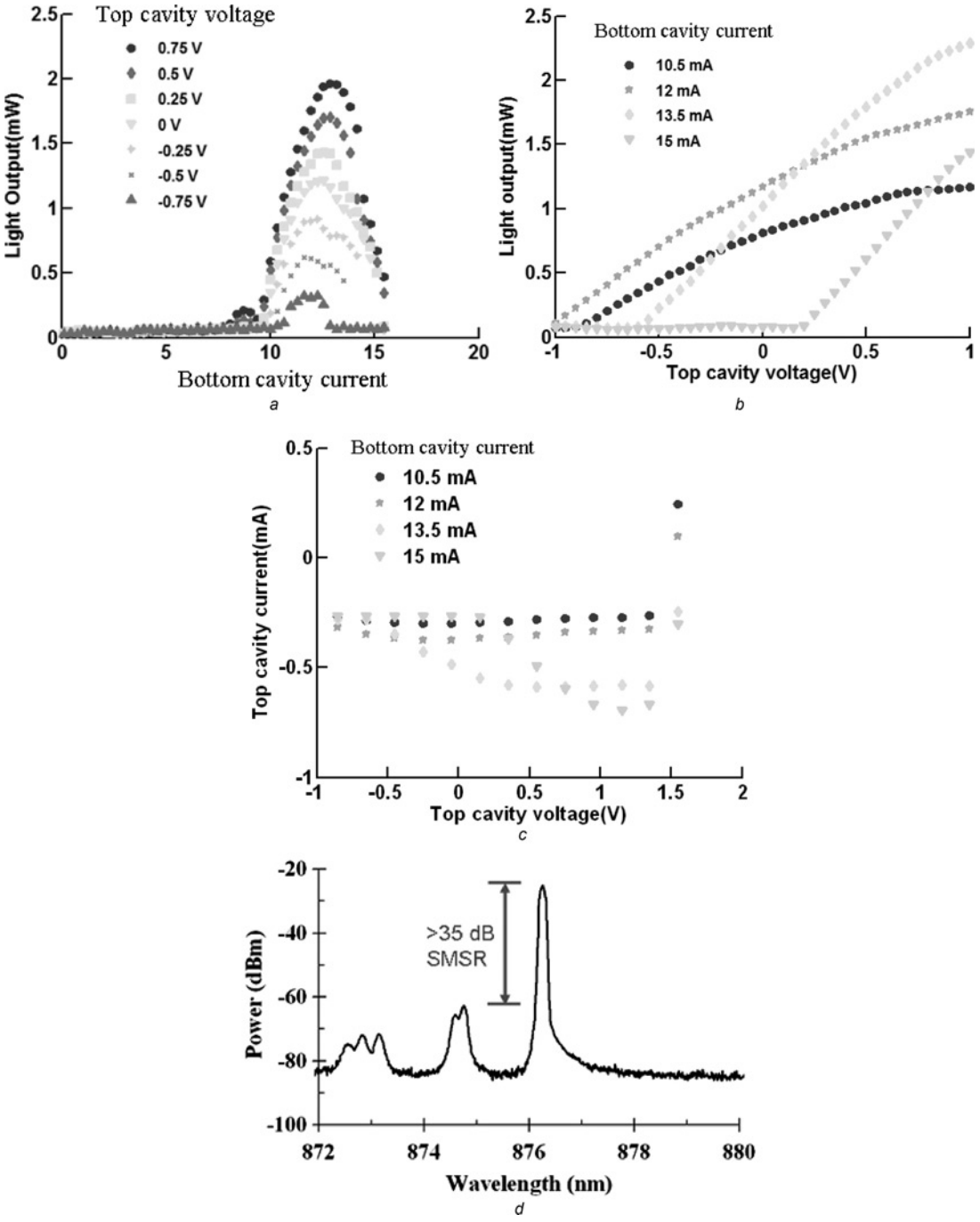

Figure 2 *CW characteristics of the CRVCL using on-wafer probing at room temperature*

a Light output against bottom cavity current for different voltages across the top cavity
b Light output power against voltage applied to the top cavity at different current injection levels into the bottom cavity
c Current against voltage in the top cavity at different current injection levels to the bottom cavity
d Optical spectrum of the CRVCL when the bottom cavity current is 12 mA

The wavelength shift from the cold-cavity resonance at 869.5 nm in the reflectance spectrum is because of device heating. As the reverse voltage increases in the top cavity, the excitonic absorption peak shifts towards the lasing wavelength, causing higher loss and thus higher threshold current to the CRVCL.

For high-speed measurements, both the small- and large-signal modulation characteristics of the CRVCL are obtained. The CRVCL is contacted on-wafer through a ground-signal–ground high-speed coplanar probe, and the light output is carefully coupled to a cleaved-optical fibre probe and then received by a high-speed photodetector. In the small-signal measurement, the top cavity receives the dc voltage from a voltage source plus a small-signal voltage modulation from a vector network analyser (VNA), whereas the bottom cavity receives the dc current only from

a second current source. The electroabsorption modulation response of the CRVCL is obtained from the S-parameter measurement on the VNA. A similar setup is also used in the large-signal measurement, where the top cavity receives a large signal directly from a bit error rate tester and the output from the high-speed photodetector is connected to a high-speed oscilloscope.

3 Analysis

In order to calculate the small-signal response of the CRVCL under electroabsorption modulation, the standard rate equations for carrier and photon densities are used [22]

$$\frac{dN}{dt} = \frac{\eta_i J}{qd} - \frac{N}{\tau} - vg(N)S \tag{1}$$

$$\frac{dS}{dt} = \Gamma vg(N)S - \frac{S}{\tau_p} + \beta R_{sp} \tag{2}$$

where N is the carrier density (cm^{-3}), η_i the current injection efficiency, J the current density (A/cm^2), q the elementary charge (C), d the gain region thickness (cm), τ the carrier lifetime (s), v the group velocity of light in the material (cm/s), $g(N)$ the gain coefficient, S the photon density (cm^{-3}), Γ the optical confinement factor, β the spontaneous emission factor and R_{sp} the spontaneous emission rate per unit volume ($cm^{-3}\,s^{-1}$). In this analysis, we do not separate the contribution from each cavity as in [16, 23]. In (2), τ_p is the photon lifetime (s) and is related to the absorption loss of a laser by

$$\frac{1}{\tau p} = v(\alpha_m + \alpha_i) = v\alpha \tag{3}$$

where α_m and α_i correspond to the mirror loss and intrinsic loss, respectively, and they are lumped into a single term α for simplicity. Therefore (2) becomes

$$\frac{dS}{dt} = \Gamma vgS - v\alpha S + \beta R_{sp} \tag{4}$$

For small-signal analysis, the equations for the total photon density, carrier density and absorption loss are given in (5), (6), and (7), respectively, as

$$S(t) = S_0 + s(t) \tag{5}$$

$$N(t) = N_0 + n(t) \tag{6}$$

$$\alpha(t) = \alpha_0 + \alpha(t) \tag{7}$$

Here we consider the CRVCL undergoes modulation of absorption loss through voltage modulation of one of its cavities. Similar to [19, 23], the small-signal variations $s(t)$, $n(t)$ and $\alpha(t)$ are assumed to be very small compared with their steady-state counterparts S_0, N_0 and α_0. Assume that $s(t)$, $n(t)$ and $\alpha(t)$ are sinusoidally varying functions, they can be described as

$$s(t) = \mathrm{Re}[(s(\omega)e^{-i\omega t}] \tag{8}$$

$$n(t) = \mathrm{Re}[(n(\omega)e^{-i\omega t}] \tag{9}$$

$$\alpha(t) = \mathrm{Re}[(\alpha(\omega)e^{-i\omega t}] \tag{10}$$

Consequently, the rate equations (1) and (4) can be solved to yield the modulation response of the CRVCL under absorption modulation

$$\left|\frac{s(\omega)}{v_{top}(\omega)}\right| = AS_0 v \frac{\sqrt{\omega^2 + \gamma^2}}{\sqrt{(\omega^2 - \omega_r^2)^2 + \omega^2\gamma^2}} \tag{11}$$

Note that $v_{top}(\omega)$ represents the small-signal top-cavity voltage and assume that it is linearly related to $\alpha(\omega)$ with a constant A, that is, $v_{top}(\omega) = A\alpha(\omega)$. In (11), the relaxation oscillation (RO) frequency $f_r = \omega_r/2\pi$ and the damping factor γ can be approximated by

$$f_r = \frac{1}{2\pi}\sqrt{vg'\frac{S_0}{\tau_p}} \tag{12}$$

$$\gamma = \frac{1}{\tau} + vg's_0\left(1 + \frac{\varepsilon}{vg'\tau_p}\right) \tag{13}$$

where g' is the differential gain and ε the gain suppression coefficient to account for nonlinear gain saturation. Similar to the modulation response because of current modulation, (11) suggests that the CRVCL under absorption modulation should also experience an RO peak. However, this RO peak should rise more rapidly but damp more slowly owing to the term $\sqrt{\omega^2 + \gamma^2}$ in the numerator of (11).

4 Results

Fig. 3*a* illustrates the small-signal modulation response of the CRVCL at different dc voltage biases across the top cavity, whereas the current to the bottom cavity is held at 12 mA. The lines are the measured data taken with 20 averages, a smooth factor of 10% and normalised to 0 dB at dc. The maximum −3 dB modulation bandwidth is 12.5 GHz, when the dc voltage across the top cavity is 0 V. The RO frequencies of the modulation response vary slightly at different dc voltage levels. As (12) predicted the decreased photon density results in a lower RO frequency. Therefore the CRVCL with a larger reverse voltage bias across the top cavity has lower light output because of increasing absorption loss, and thus it has a lower RO frequency as expected. Fig. 3*b* illustrates the small-signal modulation response of the CRVCL at a variety of current injection levels to the bottom cavity, whereas the dc voltage bias across the top cavity is held at −0.2 V. Note that the RO frequency again varies at different current injection levels,

doi: 10.1049/iet-opt.2007.0095

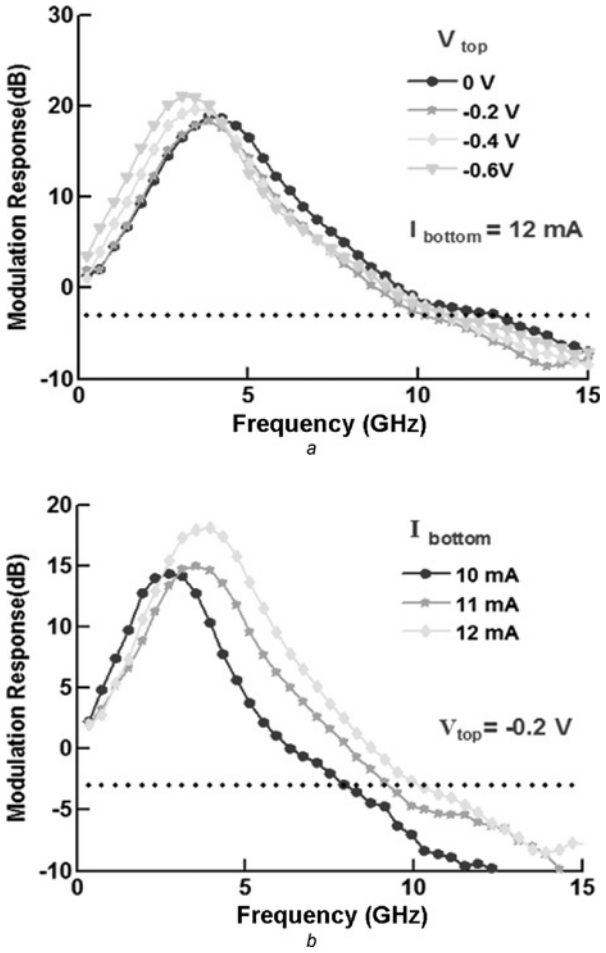

Figure 3 *Small-signal modulation response of the CRVCL at different dc voltage biases*

a Measured small-signal modulation response of a CRVCL under electroabsorption modulation at different top cavity voltages. The current injection into the bottom cavity is 12 mA

b Measured small-signal modulation response of a CRVCL under electroabsorption modulation at different bottom cavity current levels. The voltage across the top cavity is −0.2 V

because the light output from the CRVCL increases as more current is injected to the bottom cavity. In addition, the −3 dB modulation bandwidth extends to higher frequency as the RO frequency increases.

Fig. 4 shows the calculated modulation response of the CRVCL using (11)–(13). Some of the important device parameters used in the calculation are summarised in Table 1 [24]. The value of the photon density S_0 is chosen so that the light output power of the CRVCL is 1 mW and the RO frequency is similar to that in Fig. 3*a*. As mentioned earlier, the theoretical −3 dB modulation bandwidth can extend to a much higher frequency because of the slower damping of the RO peak. However, in reality the −3 dB modulation bandwidth will be limited by parasitic effects. For the CRVCL in this work, parasitic effects are primarily because of series resistance, capacitance between the contact pads and junction capacitance of the top cavity. The series resistance is 60 Ω and the total shunt

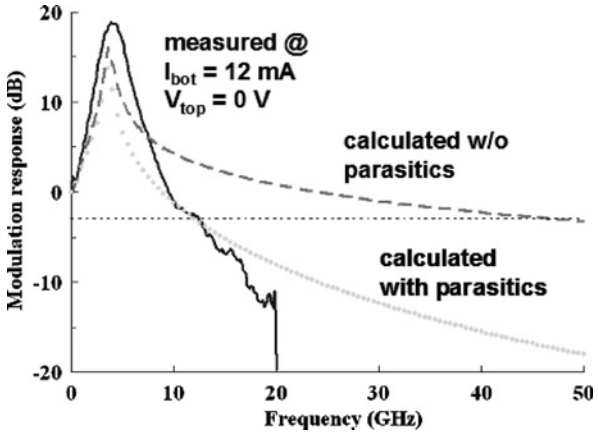

Figure 4 *Calculated modulation response of a CRVCL under intracavity electroabsorption modulation without parasitic effects (solid curve) and with parasitic effects (dashed curve)*

Table 1 Device parameters for modulation response calculation

v, cm/s	$3/3.5 \times 10^{10}$
τ, ns	2.6
τ_p, ps	2.5
g', cm^{-2}	5×10^{-16}
ε, cm^3	1.5×10^{-17}
S_0, cm^{-3}	3×10^{14}

capacitance under reverse voltage bias is 1.5 pf measured with a capacitance meter. Therefore (11) is modified to the following form to account for parasitic effects

$$\left|\frac{s(\omega)}{v_{\text{top}}(\omega)}\right| = AS_0 v \frac{\sqrt{\omega^2+\gamma^2}}{\sqrt{(\omega^2-\omega_r^2)^2+\omega^2\gamma^2}} \frac{1}{\sqrt{1+(\omega/\omega_{RC})^2}} \tag{14}$$

where ω_{RC} can be determined from the RC constant. The calculated modulation response of the CRVCL including the measured parasitic effects shown in Fig. 4 exhibits the same maximum −3 dB modulation bandwidth as that in Fig. 3*a*.

The CRVCL in this work is not an optimum design for the high-speed operation under electroabsorption modulation. For example, the upper mesa containing the top cavity with a dimension of $40 \times 40\ \mu m^2$ has a relatively large junction capacitance. In addition, the electrical contacts across the thick top and middle DBR mirrors also result in a large series resistance. Even though the CRVCL under electroabsorption modulation shows great potential to achieve higher modulation frequency than that using the conventional direct modulation, deployment into the traditional analog and digital–optical links will be

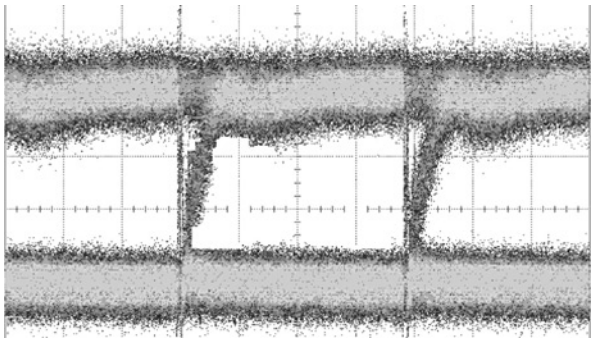

Figure 5 *Large-signal modulation eye diagram (unfiltered) taken at 54 Mbps*

difficult, because of the large RO peak in the modulation response. To illustrate this, large-signal modulation was measured and Fig. 5 shows an eye diagram taken at 54 Mbps. Unfortunately, the CRVCL cannot be modulated at a higher bit rate in spite of its 12.5 GHz small-signal bandwidth. The electroabsorption modulation represents a different paradigm of laser modulation by having higher modulation bandwidth, yet a larger RO peak when compared with that of the conventional direct modulation. Possible solutions can be pursued to flatten the modulation response and thus enable it to modulate at higher data rates [20, 25].

5 Conclusion

The CRVCL is fabricated and its characteristics under high-speed electroabsorption modulation are reported. Compared with the conventional VCSEL, the flexibility of the CRVCL allows its light output to be varied by modulating the voltage across one of its cavities. The high-speed characteristics of the CRVCL are obtained in both the small- and large-signal modulation measurements. The maximum −3 dB small-signal modulation bandwidth of 12.5 GHz is measured. The electroabsorption modulation response of the CRVCL is derived from the standard rate equations, and the calculated modulation response is in quantitative agreement with the measured one. With an optimum design, the CRVCL exhibits the potential to achieve higher modulation bandwidth than that of a conventional VCSEL. However, the large-signal modulation of the CRVCL is limited to low bit rates because of the pronounced relaxation oscillation resonance response. Future investigation of approaches that flatten or avoid the RO peak would make the CRVCL an attractive light source in the future high-speed optical links.

6 Acknowledgment

A. Allerman at Sandia National Laboratories, in Albuquerque, New Mexico, USA, is acknowledged for the epitaxial materials.

7 References

[1] CHOQUETTE K.D., GEIB K.M.: 'Fabrication and performance of vertical-cavity surface-emitting lasers', in WILMSEN C., TEMKIN H., COLDREN L. (EDS.): 'Vertical-cavity surface-emitting lasers' (Cambridge University Press, New York, 1999), pp. 193–232

[2] TSANG W.T.: 'The cleaved-couple-cavity laser', in 'Semiconductors and semimetals' (Academic Press, Orlando, FL, 1985), pt. B, vol. 22, pp. 257–373

[3] SUEMATSU Y., YAMADA M., HAYASHI K.: 'Integrated twin-guide Al–GaAs laser with multiheterostructure', *IEEE J. Quant. Electron.*, 1975, **QE-11**, pp. 457–460

[4] COLDREN L.A., MILLER B.I., IGA K., RENTCHLER J.A.: 'Monolithic two-section GaInAsP/InP active-optical-resonator devices formed by reactive ion etching', *Appl. Phys. Lett.*, 1981, **38**, pp. 315–317

[5] STANLEY R.P., HOUDRE R., OESTERLE U., ILEGEMS M., WEISBUCH C.: 'Coupled semiconductor microcavities', *Appl. Phys. Lett.*, 1994, **65**, (16), pp. 2093–2095

[6] PELLANDINI P., STANLEY R.P., HOUDRE R., *ET AL.*: 'Dual wavelength laser emission from a coupled semiconductor microcavity', *Appl. Phys. Lett.*, 1997, **71**, (7), pp. 864–866

[7] FISCHER A.J., CHOQUETTE K.D., CHOW W.W., HOU H.Q., GEIB K.M.: 'Coupled-resonator vertical-cavity laser diode', *Appl. Phys. Lett.*, 1999, **75**, (19), pp. 3020–3022

[8] FISCHER A.J., CHOQUETTE K.D., CHOW W.W., *ET AL.*: 'Q-switched operation of coupled-resonator vertical-cavity laser diode', *Appl. Phys. Lett.*, 2000, **76**, (15), pp. 1975–1977

[9] BRUNNER M., GULDEN K., MOSER M., *ET AL.*: 'Continuous-wave dual-wavelength lasing in a two-section vertical-cavity laser', *IEEE Photon. Technol. Lett.*, 2000, **12**, pp. 1316–1318

[10] FISCHER A.J., CHOQUETTE K.D., CHOW W.W., ALLERMAN A.A., GEIB K.M.: 'Bistable output from a coupled-resonator vertical-cavity laser diode', *Appl. Phys. Lett.*, 2000, **77**, (21), pp. 3319–3321

[11] FISCHER A.J., CHOQUETTE K.D., CHOW W.W., *ET AL.*: 'High single-mode power observed from a coupled-resonator vertical-cavity laser diode', *Appl. Phys. Lett.*, 2001, **79**, (25), pp. 4079–4081

[12] GRASSO D.M., CHOQUETTE K.D.: 'Threshold and modal characteristics of composite-resonator vertical-cavity lasers', *IEEE J. Quant. Electron.*, 2003, **39**, (12), pp. 1526–1530

[13] YOUNG E.W., GRASSO D.M., LEHMAN A.C., CHOQUETTE K.D.: 'Dual channel wavelength division multiplexing output using a composite-resonator vertical-cavity laser', *IEEE Photon. Technol. Lett.*, 2004, **16**, pp. 966–968

doi: 10.1049/iet-opt.2007.0095

[14] GRASSO D.M., CHOQUETTE K.D.: 'Temperature-dependent polarization characteristics of composite-resonator vertical-cavity surface-emitting lasers', *IEEE J. Quant. Electron.*, 2005, **41**, (2), pp. 127–131

[15] GRASSO D.M., CHOQUETTE K.D., SERKLAND D.K., PEAKE G.M., GEIB K.M.: 'High slope efficiency measured from a composite-resonator vertical-cavity laser', *IEEE Photon. Technol. Lett.*, 2006, **18**, (9), pp. 1019–1021

[16] GRASSO D.M., SERKLAND D.K., PEAKE G.M., GEIB K.M., CHOQUETTE K.D.: 'Direct modulation characteristics of composite-resonator vertical-cavity lasers', *IEEE J. Quant. Electron.*, 2006, **42**, (12), pp. 1248–1254

[17] LEHMAN A.C., CHOQUETTE K.D.: 'Threshold gain temperature dependence of composite-resonator vertical-cavity lasers', *IEEE J. Sel. Top. Quant. Electron.*, 2005, **11**, (5), pp. 962–967

[18] PARASKEVOPOULOS A., HENSEL H.-J., MOLZOW W.-D., *ET AL.*: 'Ultra-high-bandwidth (>35 GHz) electrooptically modulated VCSEL'. Optical Fiber Communication Conf. (PDP22), Anaheim, CA, March 2006

[19] VAN EISDEN J., YAKIMOV M., TOKRANOV V., *ET AL.*: 'Modulation properties of VCSEL with intracavity modulator', in CHOQUETTE K.D., GUENTER J.K. (EDS.): Vertical-cavity surface-emitting lasers IX, *Proc. SPIE*, 2007, **6484**

[20] VAN EISDEN J., YAKIMOV M., TOKRANOV V., *ET AL.*: 'Optical decoupling in a loss-modulated duo-cavity VCSEL'. 2007 Conf. Lasers and Electro Optics, Baltimore, MD, May 2007

[21] SHCHUKIN V.A., LEDENTSOV N.N., LOTT J.A., *ET AL.*: 'Ultra high-speed electro-optically modulated VCSELs: modeling and experimental results', *Proc. SPIE*, 2008, **6889**

[22] CHUANG S.L.: 'Physics of optoelectronic devices' (Wiley, New York, 1995)

[23] BADILITA V., CARLIN J.F., ILEGEMS M., PANJOTOV K.: 'Rate-equation model for coupled-cavity surface-emitting lasers', *IEEE J. Quant. Electron.*, 2004, **40**, pp. 1646–1656

[24] COLDREN L.A., CORZINE S.W.: 'Diode lasers and photonic integrated circuits' (Wiley, New York, 1995)

[25] AVRUTIN E.A., GORFINKEL V.B., LURYI S., SHORE K.A.: 'Control of surface-emitting laser diodes by modulating the distributed Bragg mirror reflectivity: small-signal analysis', *Appl. Phys. Lett.*, 1993, **63**, (18), pp. 2460–2462